Materials Horizons

ROYAL SOCIETY OF CHEMISTRY

COMMUNICATION

View Article Online
View Journal

Cite this: DOI: 10.1039/d5mh01902h

Received 7th October 2025,
Accepted 10th April 2026

DOI: 10.1039/d5mh01902h

rsc.li/materials-horizons

Reprogrammable shape memory ion gels *via* physical entanglement of ultrahigh molecular weight polymers

Ryota Tamate, *[ab] Koichiro Uto, *[a] Yuji Kamiyama [a] and Takeshi Ueki [ac]

In this study, we develop shape memory ion gels comprising ultrahigh molecular weight (UHMW) polymers and ionic liquids (ILs), synthesised *via* a facile one-pot radical polymerisation method of vinyl monomers in the IL medium. The resulting ion gels exhibit a high glass transition temperature (T_g) above room temperature and a broad rubbery plateau, attributed to the abundant physical entanglements of the UHMW polymers in the IL medium. Dynamic mechanical analysis confirms their excellent shape-memory performance, including triple shape-memory behaviour. By leveraging the nonvolatility of IL, the ion gels can be recycled through thermal remoulding with minimal degradation in their mechanical properties. Furthermore, they retain their shape-memory performance over multiple deformation cycles with negligible residual strain, in contrast to their counterparts containing lower molecular weight polymers, which suffer from chain pullout and incomplete recovery. Notably, this study demonstrates that densely entangled polymer networks can enable shape reprogramming, highlighting physical entanglements as a robust and dynamic cross-linking motif. Moreover, the T_g can be finely tuned by adjusting the polymer/IL composition or by selecting different IL structures, offering a versatile strategy for designing high-performance shape memory materials.

New concepts

In this study, we developed reprogrammable shape memory ion gels composed of ultrahigh molecular weight polymers and ionic liquids, synthesised *via* a facile one-pot radical polymerisation method. This system offers a versatile platform for designing shape memory materials with tuneable properties by adjusting the polymer/ionic liquid ratio and the ionic liquid structure. We demonstrated that the ion gels exhibited high mechanical strength, recyclability, and excellent shape-memory performance, including triple-shape memory behaviour. Cyclic tests showed that the ion gel retained its shape-memory function over repeated use with minimal residual strain. Notably, this is the first study to report permanent shape reprogramming solely through thermal relaxation of physical entanglements. Our results challenge the conventional reliance on dynamic covalent networks for reprogrammable plasticity and establish physical entanglements as a dynamic, tuneable, and robust cross-linking motif. We believe that our study makes a significant contribution to the literature because it provides a versatile platform for next-generation shape memory materials with customizable thermal and mechanical properties, and broad applicability in smart actuators, soft robotics, and recyclable functional systems.

1. Introduction

Shape memory polymers (SMPs) are a class of smart materials capable of recovering their pre-programmed (memorized) shape upon exposure to external stimuli such as temperature, light, magnetic fields, and humidity.[1–9] This unique functionality has garnered significant attention for various applications ranging from biomedical devices and cell culture substrates to soft actuators and responsive devices.[10–18]

Thermally responsive SMPs can be broadly categorized based on their shape-memory mechanism: those governed by the melting temperature (T_m) of the polymer and those relying on the glass transition temperature (T_g).[19–21] T_m-based SMPs offer sharp and well-defined thermal responses,[22–24] while T_g-based SMPs provide the flexibility to store multiple shapes due to the broader transition range associated with T_g.[25–27] The network structures of SMPs can be established through either physical cross-links, such as hydrogen bonding, ionic interaction, and polymer chain entanglements with finite relaxation times,[28–30] or *via* chemical cross-links through multi-functional monomers or covalent bonding introduced at side-chains or chain-ends.[31–33] Although physically cross-linked SMPs offer superior mouldability, they are often susceptible to creep deformation, a limitation less pronounced in chemically cross-linked systems.

Among physically cross-linked SMPs, systems relying on chain entanglements have been extensively explored.[34,35] Notable examples include ultrahigh molecular weight (UHMW)

[a] *Research Center for Macromolecules & Biomaterials, National Institute for Materials Science, 1-2-1 Sengen, Tsukuba, 305-0047, Japan. E-mail: TAMATE.Ryota@nims.go.jp, UTO.Koichiro@nims.go.jp*
[b] *PRESTO, JST, 7 Gobancho, Chiyoda-ku, Tokyo, 102-0076, Japan*
[c] *Graduate School of Life Science, Hokkaido University, Kita 10, Nishi 8, Kita-ku, Sapporo, Hokkaido 060-0810, Japan*

polynorbornene, commercially known as Norsorex®,[36,37] as well as UHMW polyethylene and poly(methyl methacrylate) (PMMA)-grafted poly(ethylene glycol), all of which exhibit shape memory capabilities.[38–40] More recently, pioneering work by Sumerlin and co-workers reported that UHMW styrenic polymers prepared *via* controlled radical polymerisation exhibit shape-memory properties.[41] Despite the absence of chemical cross-linking points, SMPs based on UHMW polymers exhibit excellent shape-memory performance owing to the dense network of physical entanglements. However, these materials suffer from limited tunability of T_g and often require multi-step processing, including polymerisation, purification, and moulding.

We have previously reported the development of physically cross-linked polymer gels comprising entangled UHMW polymers using *in situ* radical polymerisation in ionic liquids (ILs) under extremely low initiator concentrations, referred to as UHMW ion gels.[42] Despite being free of chemical cross-linkers and composed solely of polymer chain entanglements, these gels exhibit excellent mechanical properties. Furthermore, they demonstrate outstanding self-healing abilities and recyclability due to the reversible nature of physical entanglements.

In this study, we developed reprogrammable shape memory ion gels *via* physical entanglement of UHMW polymers. By optimizing polymer chemical structures and compositions, we successfully fabricated UHMW ion gels with a readily tuneable glass transition temperature (T_g) above room temperature and a significantly wide rubbery plateau (Fig. 1a). Relaxation spectra are extracted from the viscoelastic master curves, revealing that UHMW ion gels show a pronounced separation between the relaxation peak associated with the glass transition and that associated with terminal flow behaviour. In addition, viscoelastic and thermal analyses demonstrated that the resulting ion gels exhibit a broader glass transition compared to neat PMMA and commercially available polyurethane-based SMPs.

The developed ion gels exhibited exceptionally high mechanical properties at room temperature, along with outstanding

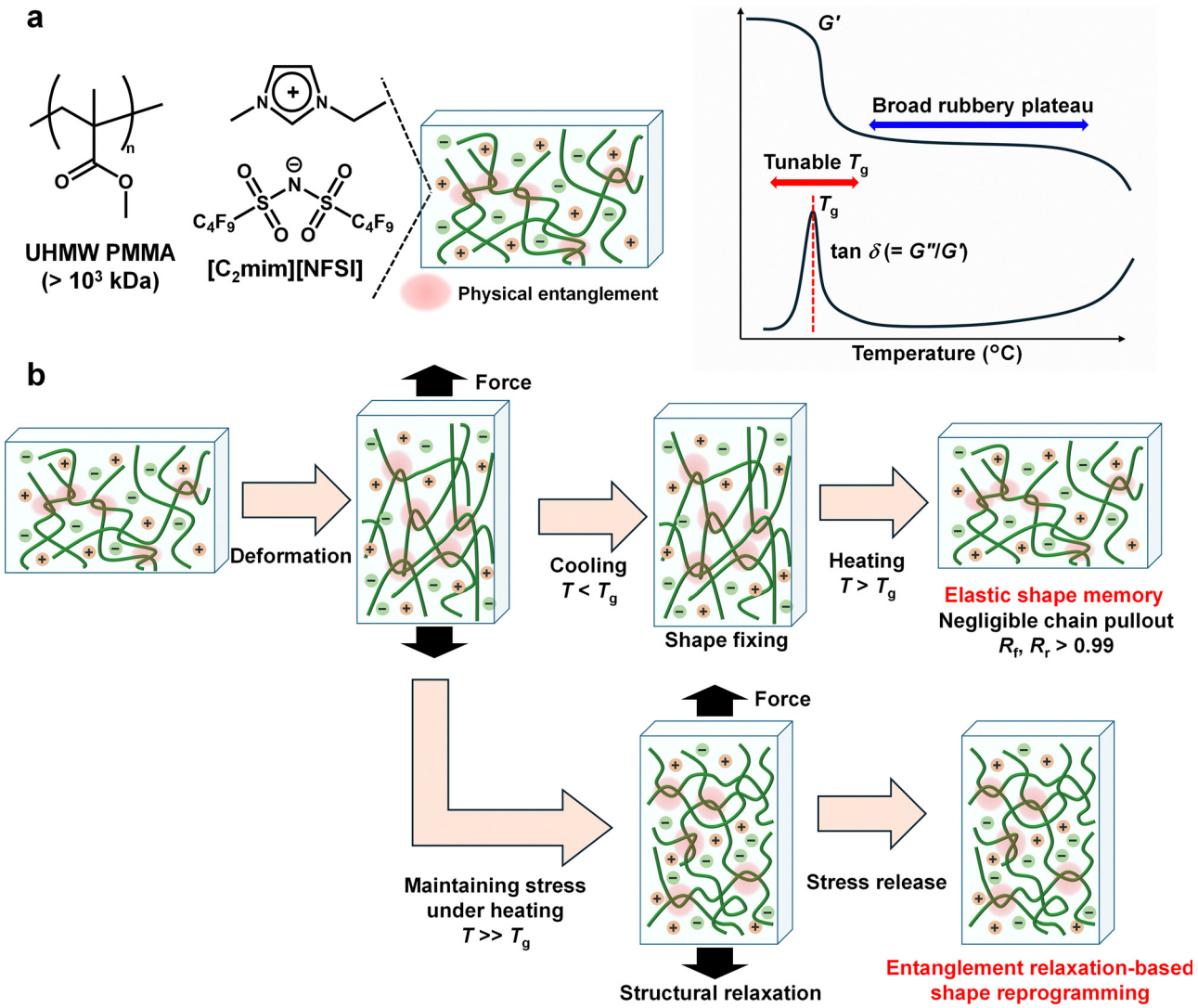

Fig. 1 (a) Chemical structures and schematic viscoelastic behaviour of the reprogrammable shape memory UHMW ion gels. (b) Schematic of the shape-memory and shape-reprogramming capabilities enabled *via* physical entanglement of UHMW polymers.

shape-memory performance, including triple shape-memory behaviour driven by polymer entanglements. Furthermore, the gels could be readily recycled through thermal moulding, leveraging the reversibility of physical entanglements and the non-volatility and high thermal stability of ILs. In addition, sensing of strain associated with shape deformation was demonstrated by exploiting the ionic conductivity of the material. Notably, this work provides the demonstration that reprogrammable multiple shape-memory behaviour can be achieved solely through dense physically-entangled polymer networks, underscoring the role of physical entanglements as both durable and adaptable cross-linking points (Fig. 1b).

2. Results and discussion

We have previously reported the synthesis of UHMW polymers with molecular weights exceeding 10^6 Da and nearly 100% monomer conversion *via* free radical polymerisation of vinyl monomers in ILs or highly concentrated lithium salt electrolytes, using minimal radical initiator concentrations.[42–45] In this study, we used methyl methacrylate (MMA) as the monomer and 1-ethyl-3-methylimidazolium bis(nonafluorobutanesulfonyl)imide ([C_2mim][NFSI]) as IL. By adjusting the monomer/IL ratio, we tuned T_g above room temperature and successfully synthesised PMMA/[C_2mim][NFSI] ion gels *via* a one-pot process, in which the entanglement of UHMW PMMA serves as the driving force for shape-memory properties. For comparison, we also synthesised composites with lower molecular weights by increasing the initiator concentration. Additionally, an UHMW ion gel was also prepared using bis(trifluoromethanesulfonyl)imide (TFSI) instead of NFSI as the anion structure. The composition of the obtained composites, the molecular weight and molecular weight distribution of PMMA, and the T_g of the composites are summarized in Table 1. The 45wt-PMMA-H-[C_2mim][NFSI] sample refers to an ion gel consisting of 45 wt% UHMW PMMA (number-averaged molecular weight $M_n > 10^3$ kDa), combined with the IL [C_2mim][NFSI]. In contrast, 45wt-PMMA-M-[C_2mim][NFSI] and 45wt-PMMA-L-[C_2mim][NFSI] denote composites incorporating relatively medium (M_n = 127 kDa) and low (M_n = 45 kDa) molecular weight PMMA, respectively. The samples 60wt-PMMA-H-[C_2mim][NFSI] and 35wt-PMMA-H-[C_2mim][NFSI] are ion gels containing UHMW PMMA at polymer concentrations of 60 and 35 wt%, respectively. Meanwhile, 45wt-PMMA-H-[C_2mim][TFSI] is an ion gel comprising 45 wt% UHMW PMMA and a different IL, [C_2mim][TFSI]. The obtained ion gels are transparent and exhibit excellent long-term stability under various conditions. Fig. S1 shows the appearance and mass change of disk-shaped 45wt-PMMA-H-[C_2mim][NFSI] ion gels after one week at room temperature, at elevated temperature (100 °C), and under compression. Under all conditions, no leakage of the IL was observed, and negligible mass change was detected.

Fig. 2a and b show the temperature dependence of the viscoelastic properties of 45 wt% PMMA/[C_2mim][NFSI] systems prepared with varying PMMA molecular weights. All samples exhibited a high storage modulus (G') of $\sim 10^8$ Pa at temperatures below room temperature, indicating a glassy state. As the temperature increased, both G' and the loss modulus (G'') decrease for all samples, with a distinct peak in the loss tangent ($\tan\delta$, G'' to G' ratio) around 50 °C, indicating the glass-to-rubber transition of the sample. Above T_g, the viscoelastic behaviour diverged significantly depending on the molecular weight of PMMA. For the 45wt-PMMA-H-[C_2mim][NFSI] sample with UHMW PMMA (M_n = 1146 kDa), G' shows a plateau up to 150 °C, revealing a very broad rubbery elastic region. In contrast, the 45wt-PMMA-M-[C_2mim][NFSI] sample with medium PMMA (M_n = 127 kDa) exhibited a crossover between G' and G'' at $\sim$136 °C, indicating the transition from the rubbery plateau to the terminal flow regime, while the 45wt-PMMA-L-[C_2mim][NFSI] sample with low PMMA (M_n = 45 kDa) barely exhibited a rubbery region. Frequency sweep measurements at different temperatures using the time-temperature superposition principle further confirmed that 45wt-PMMA-H-[C_2mim][NFSI] has a broad rubbery elastic region with no crossover between G' and G'' within the measurement range, in contrast to the 45wt-PMMA-M-[C_2mim][NFSI] sample (Fig. S2). Such results suggest that the UHMW PMMA/[C_2mim][NFSI] ion gel has a very long relaxation time due to the chain entanglement of the UHMW polymers and behaves almost similarly to a solid over extended timescales. Furthermore, relaxation spectra were calculated from the obtained viscoelastic master curves (Fig. 2c). The 45wt-PMMA-H-[C_2mim][NFSI] ion gel exhibits a relaxation peak associated with the glass transition comparable to that observed for 45wt-PMMA-M-[C_2mim][NFSI] in the short-time regime ($<10^{-2}$ s). In contrast, the relaxation peak corresponding to terminal flow differs by more than three orders of magnitude in timescale between the two samples. These results indicate that, in 45wt-PMMA-H-[C_2mim][NFSI] composed of UHMW polymers, the timescales

Table 1 The PMMA/IL composites used in this study

Name	IL structure	$c_{polymer}$[a] [wt%]	M_n[b] [kDa]	M_w[b] [kDa]	PDI[b]	T_g [°C][c]
45wt-PMMA-H-[C_2mim][NFSI]	[C_2mim][NFSI]	45	1146	1994	1.74	51
45wt-PMMA-M-[C_2mim][NFSI]	[C_2mim][NFSI]	45	127	252	1.99	50
45wt-PMMA-L-[C_2mim][NFSI]	[C_2mim][NFSI]	45	45	74	1.63	52
60wt-PMMA-H-[C_2mim][NFSI]	[C_2mim][NFSI]	60	1123	2075	1.85	75
35wt-PMMA-H-[C_2mim][NFSI]	[C_2mim][NFSI]	35	1231	2203	1.79	36
45wt-PMMA-H-[C_2mim][TFSI]	[C_2mim][TFSI]	45	1214	1982	1.63	17

[a] Concentration of PMMA in the composite. [b] Measured by GPC. [c] Determined by the peak temperature of $\tan\delta$ obtained *via* temperature sweep measurements.

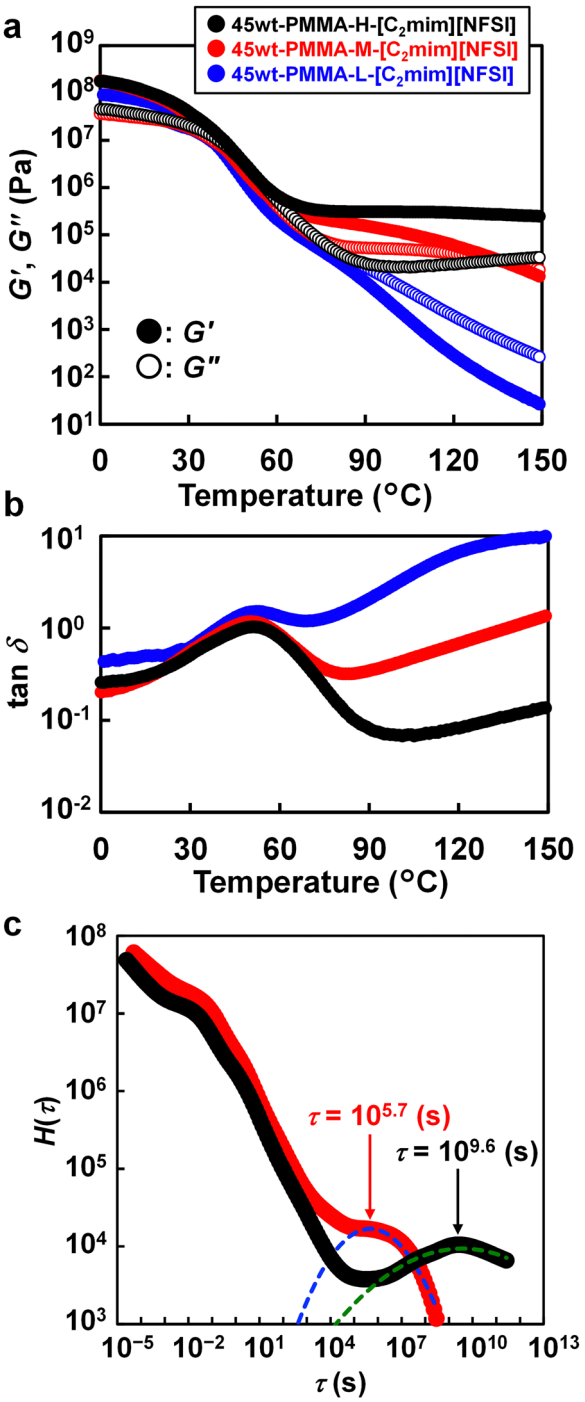

Fig. 2 (a) and (b) Temperature sweep measurements of the ion gel composed of PMMA with different molecular weights and [C_2mim][NFSI] showing the (a) storage modulus (G') and loss modulus (G'') and (b) loss tangent ($\tan\delta$). (c) Relaxation spectra of 45wt-PMMA-H-[C_2mim][NFSI] (black) and 45wt-PMMA-M-[C_2mim][NFSI] (red). The dashed curves correspond to Gaussian fits of the relaxation associated with flow deformation, and the arrows indicate the corresponding peak relaxation times.

of glass-transition-related relaxation and the terminal flow regime are well separated. Such pronounced separation likely contributes to the superior shape-memory performance of this material.

Another notable characteristic of this system is the broadening of the glass transition. Fig. S3 and Table S1 compare the temperature dependence of $\tan\delta$ for 45wt-PMMA-H-[C_2mim][NFSI] with that of neat PMMA and a commercially available polyurethane-based shape-memory polymer (KYORAKU Co., Ltd, Japan).[46,47] The 45wt-PMMA-H-[C_2mim][NFSI] ion gel exhibits a significantly broader $\tan\delta$ peak than both reference polymers. Consistently, differential scanning calorimetry (DSC) analysis shows that the onset and end temperatures of the glass transition are more widely separated for 45wt-PMMA-H-[C_2mim][NFSI], confirming a broader T_g compared to PMMA and the polyurethane-based SMP (Fig. S4a and Table S1). Such broadened glass-transition behaviour is particularly important for achieving multi-shape memory effects that exploit the extended T_g region.[48,49]

To examine whether this broad transition arises from multiple distinct transitions, modulated DSC measurements were further conducted (Fig. S4b).[50,51] The T_g determined from the reversible heat flow was nearly identical to that obtained from conventional DSC for 45wt-PMMA-H-[C_2mim][NFSI], as well as for PMMA and the polyurethane-based SMP. These results suggest that the broadened transition in 45wt-PMMA-H-[C_2mim][NFSI] originates from a single, intrinsically broadened glass transition rather than multiple transitions.

Furthermore, the shift factor a_T obtained from the time–temperature superposition master curve was well fitted by the Williams–Landel–Ferry (WLF) equation over the temperature range up to approximately T_g + 90 °C (Fig. S5). This result is consistent with the view that the viscoelastic response of the present ion gel near T_g is dominated by a single glass-transition-related relaxation process. In addition, the fragility index derived from the WLF fitting parameters was m = 61 (see the calculation details in the SI), indicating moderate fragility compared with previously reported amorphous polymeric materials.[52] Recent studies have shown that, in non-charged amorphous materials, the breadth of the relaxation spectrum generally correlates with the fragility index, whereas glassy ionic polymer complexes and poly(ionic liquid)s can exhibit broad relaxation spectra despite relatively low fragility indices.[53] In the present system, one possible origin of the broadened relaxation is a distribution of local segmental mobilities arising from polymer/IL compositing. Because the [NFSI] anion is reported to form nano-segregation of the fluorinated alkyl side chains,[54] such local dynamic heterogeneity may contribute to a broader distribution of segmental environments experienced by the PMMA chains.

Moreover, unlike conventional shape-memory materials that rely on polymer chain entanglements, this system allows facile tuning of T_g through its UHMW polymer and IL contents. Fig. S6 presents the temperature sweep measurements of UHMW PMMA/[C_2mim][NFSI] ion gels with varying polymer concentrations. The peak of $\tan\delta$ increases proportionally with the PMMA content (Table 1). Furthermore, the IL structure significantly influences T_g and other physical properties of the sample. The NFSI anion used in this study features a bulky, highly hydrophobic perfluoroalkyl chain,[55] enabling a higher T_g

at the same polymer concentration compared to the commonly used imide anion, TFSI (Fig. S7 and Table 1). ILs are often referred to as "designer solvents" because their properties can be tailored by selecting from a wide variety of cation and anion structures.[56] In addition, we have previously shown that a wide range of radically polymerisable monomers can be polymerised to ultrahigh molecular weights in ILs.[42–45] Systematic tuning of physical properties through variation of cation, anion, and monomer structures remains an important subject for future investigation.

To assess their mechanical performance, uniaxial tensile tests were conducted at room temperature on the 45 wt% PMMA/[C_2mim][NFSI] systems with different molecular weights (Fig. 3a and Table S2). All samples exhibited very high elastic moduli, with Young's moduli exceeding 100 MPa. The sample with the lowest PMMA molecular weight, 45wt-PMMA-L-[C_2mim][NFSI], did not show an increase in stress after yielding and broke at approximately 100% strain. Conversely, 45wt-PMMA-H-[C_2mim][NFSI] and 45wt-PMMA-M-[C_2mim][NFSI] exhibited a significant increase in stress after yielding, with tensile deformations exceeding 200%. 45wt-PMMA-H-[C_2mim][NFSI] exhibited a high fracture stress of approximately 22 MPa, while that of 45wt-PMMA-M-[C_2mim][NFSI] was approximately 19 MPa. During the fracture process of polymeric materials, the dominant mechanisms are thought to be main-chain scission and polymer chain pullout.[57,58] In the case of the lowest molecular weight sample, 45wt-PMMA-L-[C_2mim][NFSI], the absence of post-yield stress increase and its low fracture strain suggest fewer entanglements and polymer chain pullout dominance, leading to fracture at low strain and low stress. Conversely, 45wt-PMMA-H-[C_2mim][NFSI] and 45wt-PMMA-M-[C_2mim][NFSI] exhibited high fracture strains and stresses, suggesting that during the timescale of the tensile test, polymer chain pullout due to disentanglements was limited in these samples. Instead, fracture was primarily governed by chain scission resulting from the extension of polymer chains between entanglement points.

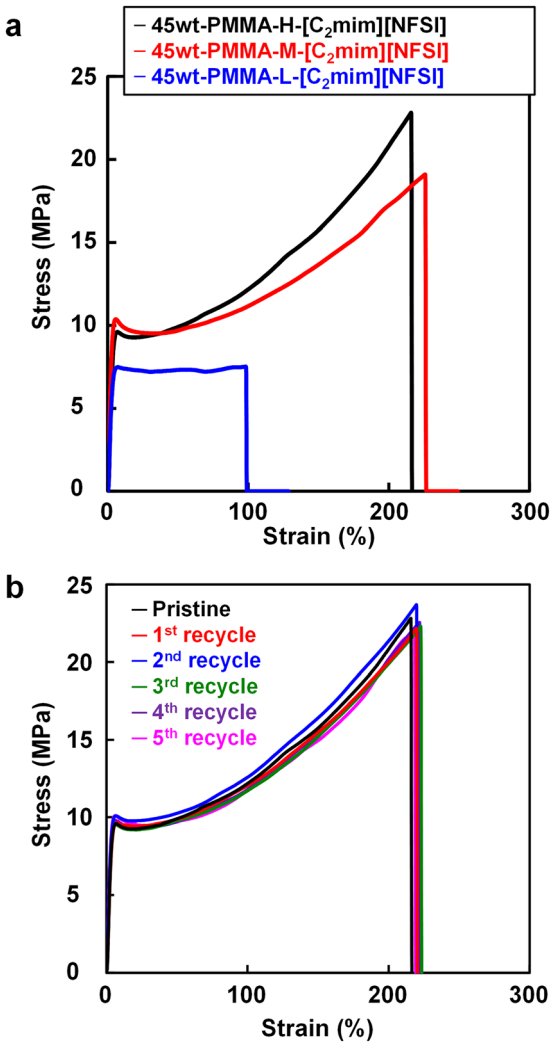

Fig. 3 (a) Uniaxial tensile tests of composites comprising PMMA with different molecular weights and [C_2mim][NFSI]. (b) Comparison of stress–strain curves between the pristine and recycled 45wt-PMMA-H-[C_2mim][NFSI] ion gels.

Furthermore, this UHMW ion gel—comprising polymer chain entanglements serving as reversible physical cross-links and an IL that acts as a non-volatile and non-flammable plasticizer[59–62]—can be recycled *via* thermal moulding. When 45wt-PMMA-H-[C_2mim][NFSI] was cut into small pieces and hot-pressed at 130 °C, the material could be re-moulded into a sheet (Fig. S8). After being punched into a dumbbell shape and subjected to tensile testing, the re-moulded sheet exhibited stress–strain characteristics similar to those of the pristine sample. Notably, even after five cycles of the recycling process, no significant changes in the tensile properties were observed, and comparable elongation at break, tensile strength, and toughness were maintained (Fig. 3b, Fig. S9, and Table S3). In addition, the viscoelastic master curves of the pristine and recycled samples were found to be nearly identical (Fig. S10). These results demonstrate that this ion gel possesses not only high mechanical strength but also repeatable recyclability. Furthermore, the present material consists of the highly hydrophobic IL [C_2mim][NFSI], containing the hydrophobic NFSI anion, and the hydrophobic polymer PMMA, which together impart excellent water resistance. Indeed, even after immersion in water for one day, the 45wt-PMMA-H-[C_2mim][NFSI] retained its transparency, and its mechanical strength remained almost unchanged (Fig. S11).

The UHMW PMMA/[C_2mim][NFSI] ion gel possesses abundant physical cross-linking points due to entanglements and exhibits a T_g above room temperature, suggesting its suitability for shape-memory applications triggered by thermal stimuli. To evaluate the shape-memory properties of the ion gel, a shape-memory test was conducted using dynamic mechanical analysis (DMA). The rectangular sheet-shaped ion gel was subjected to 100% tensile deformation at 60 °C (above T_g) and the deformation was fixed by cooling to 0 °C and equilibrating. The shape fixation rate (R_f) was determined from the change in strain upon stress release, once the system reached equilibrium at 0 °C. Furthermore, the shape recovery rate (R_r) was calculated

by measuring the extent of shape recovery upon heating to 100 °C under zero-stress conditions. 45wt-PMMA-H-[C_2mim][NFSI], composed of UHMW PMMA, exhibited exceptionally high values for both R_f and R_r (R_f, R_r > 0.99), indicating excellent shape-memory performance (Fig. 4a). In the DMA tests, even when the shape-fixing time after 100% tensile deformation was extended to 12 h, the shape recovery ratio remained extremely high (R_r = 0.99, Fig. S12). This result suggests that stress-induced creep during deformation of the ion gel below T_g is negligible under the present conditions. However, because this system relies on entanglement-derived physical cross-links rather than permanent chemical cross-linking points, potential creep over much longer time scales (months to years) should be considered, and this remains an important subject for future investigation. Notably, the 45wt-PMMA-M-[C_2mim][NFSI] composite, comprising PMMA of relatively lower molecular weight, exhibited a significantly lower R_r (0.89) despite its slightly higher elongation at break than 45wt-PMMA-H-[C_2mim][NFSI] in tensile tests (Fig. 4b). This reduction in R_r is likely attributed to partial polymer chain disentanglement during tensile deformation, which leads to incomplete shape recovery driven by entropic elasticity upon heating. These results suggest that abundant UHMW polymer entanglements effectively suppress chain disentanglement during shape deformation, thereby enabling excellent shape memory properties despite the absence of chemical cross-linking.

To further assess the durability of the mechanical properties under repeated deformation during the shape memory process, a cyclic shape memory test was conducted on 45wt-PMMA-H-[C_2mim][NFSI] using tensile testing. The sample was subjected to uniaxial tensile deformation at 150% strain at room temperature, followed by shape recovery at 100 °C (Fig. 4c). Remarkably, even after five cycles, the recovered sample consistently recovered its original shape with minimal residual strain, indicating negligible creep deformation over multiple shape-memory cycles at 150% strain (Fig. 4d). The corresponding stress–strain curve revealed that the sample sustained a stress of 12 MPa at 150% strain, demonstrating its excellent mechanical performance at room temperature (Fig. 4e). Notably, this stress–strain response remained virtually unchanged throughout the five repeated tensile cycles, suggesting that neither significant polymer chain disentanglement nor chain scission occurred during the cyclic shape-memory process. In contrast, when the same test was performed on 45wt-PMMA-M-[C_2mim][NFSI], a clear residual strain was observed after testing, and the sample exhibited incomplete shape recovery (Fig. S13). These findings further highlight the critical role of dense entanglements in UHMW polymer networks in ILs for achieving both high mechanical strength and superior shape recovery.

Next, we demonstrated actuation driven by shape recovery in a sheet sample subjected to thermal stimuli. A rectangular-shaped sheet of 45wt-PMMA-H-[C_2mim][NFSI] (weight: 0.62 g) was deformed to approximately 170% strain at a temperature above its T_g, followed by cooling to room temperature to fix the deformed shape. Subsequently, a 100-g weight was suspended from the sheet, which was then placed in an oven at 100 °C.

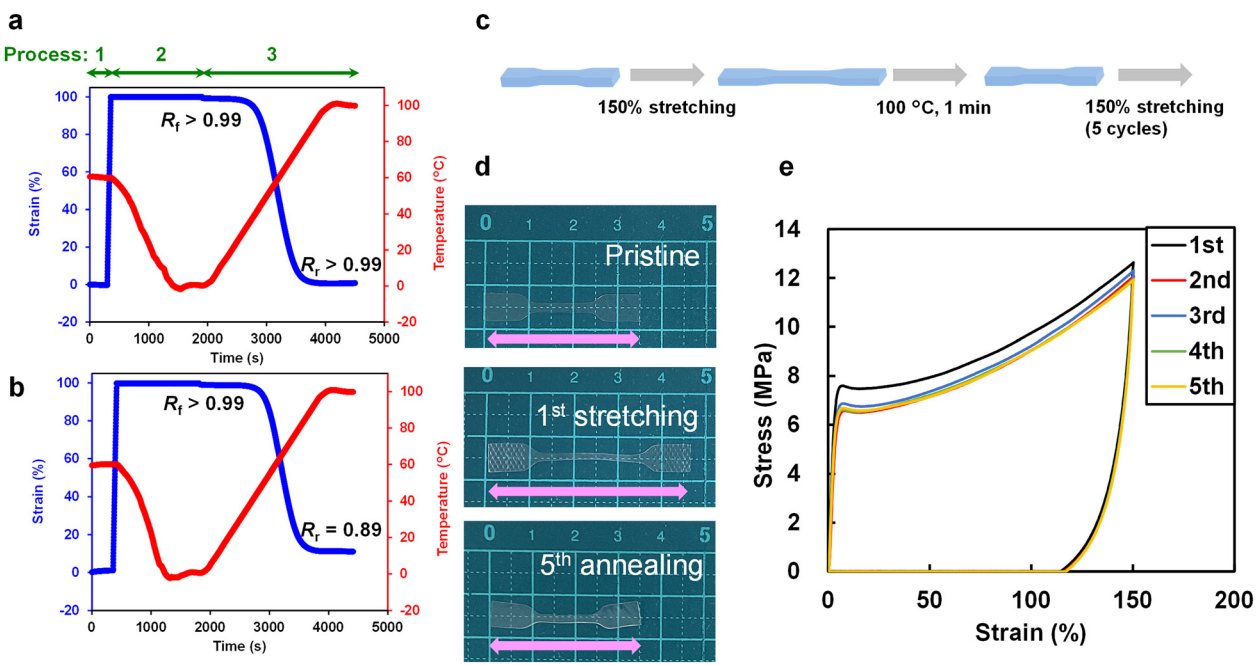

Fig. 4 (a) Shape-memory tests of 45wt-PMMA-H-[C_2mim][NFSI] and (b) 45wt-PMMA-M-[C_2mim][NFSI] measured by DMA. Process 1: deformation of the sample to 100% strain at 60 °C. Process 2: shape fixation by cooling to 0 °C while maintaining 100% strain. Process 3: shape recovery by heating to 100 °C under zero-stress conditions. The blue line represents the change in strain over time, while the red line represents the change in temperature over time. (c) Schematic of the cyclic shape memory test for 45wt-PMMA-H-[C_2mim][NFSI]. (d) Photographs of the dumbbell-shaped specimen before the test (top), after the first 150% strain (middle), and after shape recovery following the fifth cycle (bottom). (e) Stress–strain curves during 150% elongation in the repeated test.

Upon heating, the shape recovery of the sheet generated sufficient force to lift the suspended weight, clearly demonstrating its actuation capability (Fig. 5a and Movie S1). Comparison of the sheet before and after the test revealed negligible residual strain (Fig. S14), confirming that the UHMW PMMA/[C_2mim][NFSI] ion gel exhibits high shape recovery performance even under load. In a separate demonstration, a rectangular-shaped sheet was deformed into a helical configuration at elevated temperature and then cooled to fix the structure. When reheated to 100 °C, the helical-shaped sample gradually unfolded, returning to its original straight form (Fig. 5b and Movie S2). The post-test sample retained a shape nearly identical to its original, further confirming the excellent shape-memory properties of the UHMW ion gel (Fig. S15). To quantitatively evaluate the work density associated with shape recovery, loading–unloading tensile tests were performed according to a previously reported method (Fig. S16).[63] The 45wt-PMMA-H-[C_2mim][NFSI] ion gel exhibited a high work density of 2629 kJ m^{-3}. Although direct comparison of work density values should be approached with caution due to variations in evaluation methods among different studies, the present material nevertheless demonstrates outstanding work density relative to previously reported shape-memory polymers and gels (Table S4).

Above T_g, the ion gel shows a reasonably high conductivity (Fig. S17), highlighting its potential for applications such as strain sensors utilizing resistance changes induced by actuation. To examine this possibility, the bulk resistance of the ion gel was measured as a function of tensile strain at 80 °C. Fig. S18a shows that the resistance increased proportionally with increasing elongation ratio. As a demonstration, a 100% ion gel sheet was stretched at 80 °C and its resistance was recorded,

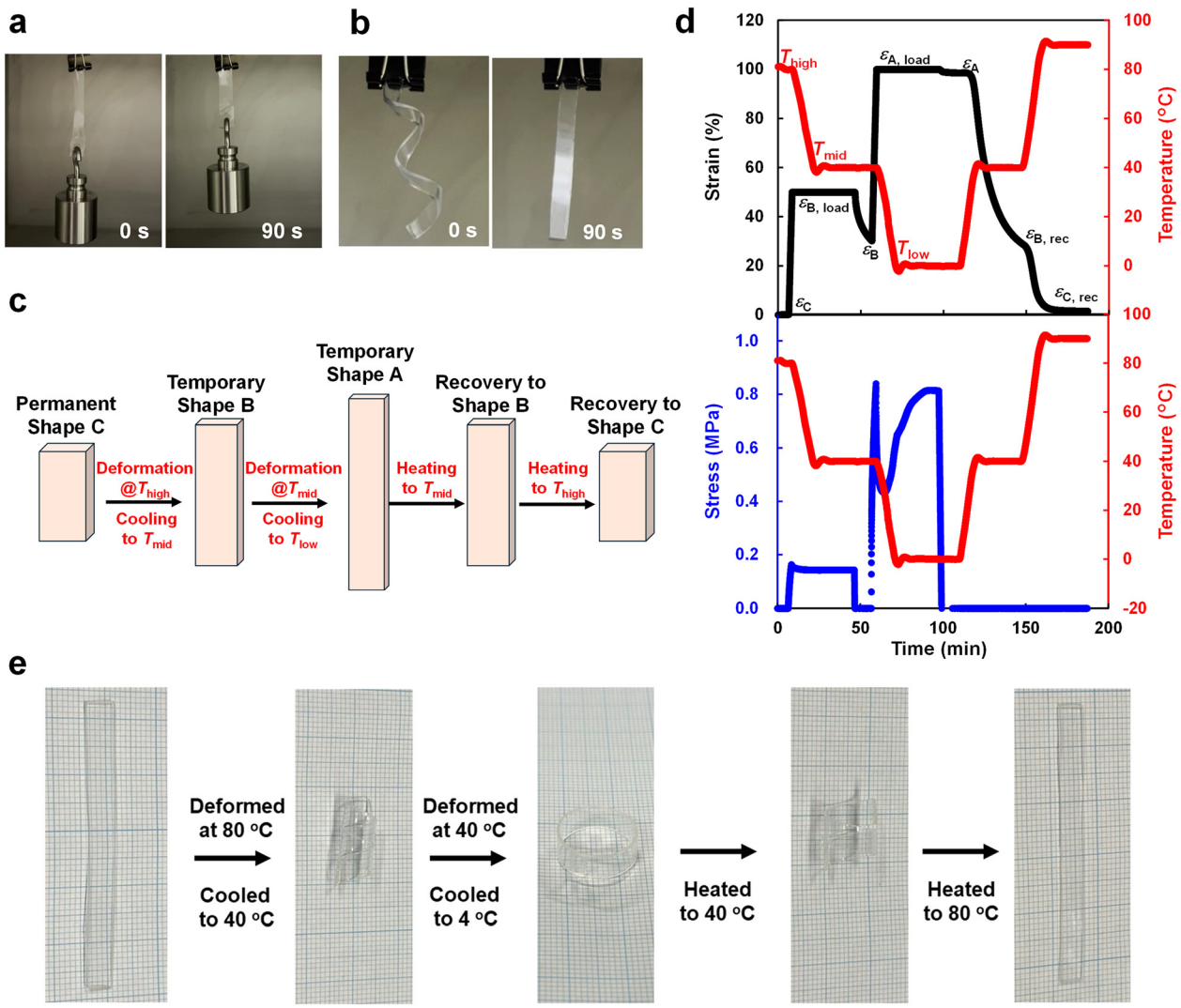

Fig. 5 (a) Snapshots of the actuation demonstration of a 45wt-PMMA-H-[C_2mim][NFSI] sheet at 0 and 90 s in the oven. (b) Snapshots of the shape transformation demonstration of a helical-shaped 45wt-PMMA-H-[C_2mim][NFSI] sheet at 0 and 90 s in the oven. (c) Schematic of TSCP by DMA. (d) Quantitative evaluation of TSCP by DMA for the 45wt-PMMA-H-[C_2mim][NFSI] ion gel. The upper graph shows the changes in temperature and strain during TSCP, while the lower graph shows the changes in temperature and stress. (e) Visual demonstration of TSCP for the 45wt-PMMA-H-[C_2mim][NFSI] ion gel, showing shape transition among a strip, a helix, and a circle.

followed by unloading to allow shape recovery. The stretching–recovery process was then repeated once more, and the resistance change was monitored. Reversible changes in bulk resistance were clearly observed during the cyclic deformation (Fig. S18b), suggesting that the shape-memory material developed in this study can exploit its ionic conductivity to sense strain changes associated with actuation through variations in bulk resistance.

Furthermore, since this material exhibits shape-memory behaviour based on the remarkably broad glass transition, it benefits from a broader transition range than melting-point-based systems and is thus expected to support multi-shape programmability. To verify this, a triple-shape creation process (TSCP) was conducted by DMA.[22,27,64] In this process, two sub-T_g temperatures were designated as shape-fixing temperatures, and the following three-step shape-memory process was conducted (Fig. 5c): Starting from the initial shape C (zero-strain state, ε_C = 0%), the sample was heated to T_{high} = 80 °C ($> T_g$) and stretched to a strain of $\varepsilon_{B,\,load}$ = 50% under load. It was then cooled to T_{mid} = 40 °C ($< T_g$) and unloaded to fix shape B with a strain of ε_B. Subsequently, it was further stretched to $\varepsilon_{A,\,load}$ = 100% at T_{mid}, followed by cooling to T_{low} = 0 °C ($< T_{mid}$) and unloading to fix shape A with a strain of ε_A. Finally, the sample was reheated to T_{mid} to recover shape B (strain: $\varepsilon_{B,\,rec}$), and then to T_{high} to recover shape C (strain: $\varepsilon_{C,\,rec}$). The result of the TSCP measured by DMA is shown in Fig. 5d. After unloading, the strain for shape A was ε_A = 98.5%, for shape B ε_B = 30.1%, for the recovered shape B $\varepsilon_{B,\,rec}$ = 29.2%, and for the recovered shape C $\varepsilon_{C,\,rec}$ = 1.5%, indicating excellent triple-shape memory performance. For shape B fixed at the intermediate temperature T_{mid}, relaxation was not fully completed. When the holding time was extended from 30 min to 150 min, the recovered shape stabilized at approximately 14% (Fig. S19). Therefore, caution is required for applications that demand strict shape fidelity. In contrast, when T_{mid} was lowered from 40 °C to 35 °C, the recovered shape after 150 min was maintained at around 31% (Fig. S20). Thus, the intermediate-temperature shape can also be controlled by tuning T_{mid}.

As a visual demonstration, Fig. 5e shows the result of TSCP where a strip shape was fixed as shape C, a helical shape as shape B, and a circular shape as shape A. Upon stepwise heating after the shape-memory process, sequential shape recovery from the circular form to the helical form and finally to the strip form was successfully observed.

Inspired by advanced shape memory systems that achieve permanent shape reprogramming *via* thermally exchangeable covalent bonds,[65] we further explored whether similar reprogramming could be realised in our system by leveraging the relaxation of physical entanglements in the UHMW polymers. To explore this possibility, we conducted a series of three shape-memory cycles, demonstrating that permanent shape transformation is indeed achievable in the UHMW PMMA/[C_2mim][NFSI] ion gel through high-temperature entanglement relaxation (Fig. 6 and Fig. S21). In Cycle 1, the sample was stretched to 25% strain at 60 °C, cooled to 0 °C to fix the temporary shape, and then reheated to 60 °C, resulting in

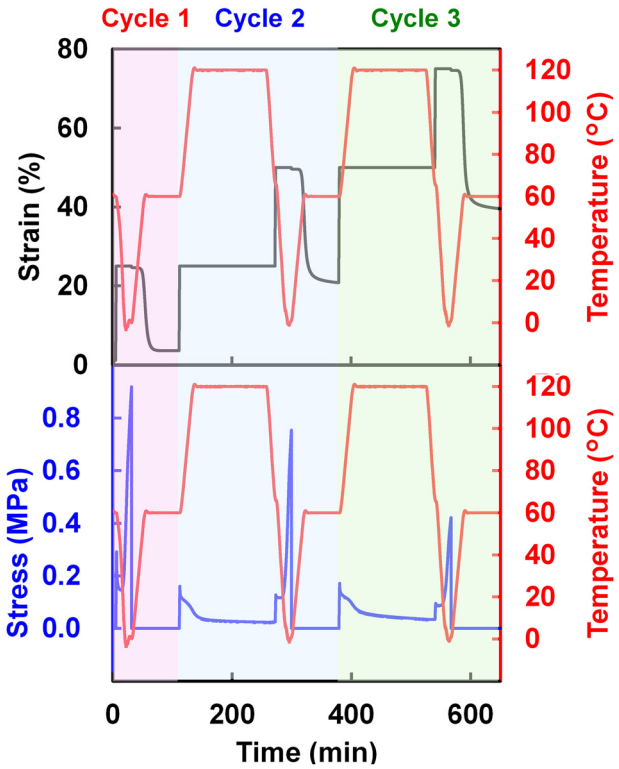

Fig. 6 Shape-reprogramming tests for 45wt-PMMA-H-[C_2mim][NFSI] through consecutive shape memory tests and thermal treatments. The upper graph shows the changes in temperature and strain over time during the shape-reprogramming process, while the lower graph shows the changes in temperature and stress.

complete shape recovery and confirming conventional thermally-induced shape-memory behaviour. In Cycle 2, we attempted permanent shape reprogramming by first applying 25% strain at 60 °C, followed by heating to 120 °C while maintaining the deformation. After this thermal treatment, the sample was further stretched to 50% strain at 60 °C, cooled to 0 °C to fix the new shape, and reheated to 60 °C. Upon reheating, the sample recovered to approximately 20% strain, indicating successful shape reprogramming, as the original shape was erased and replaced by the newly-programmed shape. In Cycle 3, further reprogramming was achieved by stretching the sample to 50% strain at 60 °C, followed by heating to 120 °C. The sample was deformed to 75% strain at 60 °C, cooled to 0 °C to fix the shape, and reheated to 60 °C, leading to recovery to approximately 40% strain. Taken together, these results demonstrate that permanent shape reprogramming can be realised in our entanglement-based UHMW ion gel by controlled thermal equilibration, in which relaxation of physical entanglements resets the permanent shape.

Based on the above results, a shape-reprogramming demonstration was conducted. A strip-shaped 45wt-PMMA-H-[C_2mim]-[NFSI] sheet was wound around a Teflon rod and fixed into a helical shape. To induce shape reprogramming, the sample underwent thermal treatment at 120 °C for 2 h. As a control, a second sample was similarly fixed in the helical shape but maintained at room temperature for the same duration. Upon

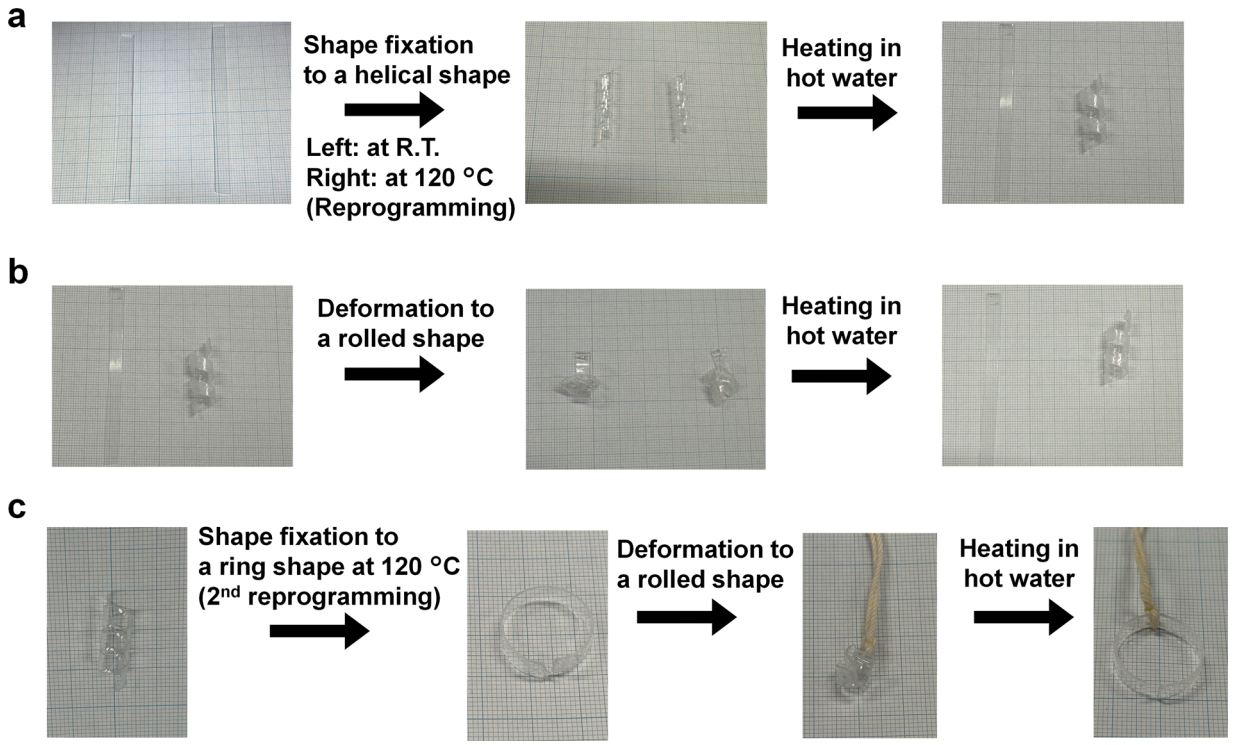

Fig. 7 (a) Demonstration of shape reprogramming from a strip shape to a helical shape for 45wt-PMMA-H-[C_2mim][NFSI]. The right sample was reprogrammed into a helical shape by fixing it at 120 °C for 2 h. The left sample is the control experiment, where the helical shape was fixed at room temperature. (b) Shape memory tests for the reprogrammed and control samples. Both samples were temporarily deformed into a rolled shape, cooled in cold water to fix the temporary shape, and then immersed in hot water. (c) Second shape reprogramming test, where the helical-shaped sample was reprogrammed into a ring shape, followed by a shape memory test in which the sample was temporarily deformed into a rolled shape and then immersed in hot water.

immersion in hot water, the control sample reverted to its original strip shape, whereas the reprogrammed sample retained its helical configuration, demonstrating successful permanent shape reconfiguration (Fig. 7a and Movie S3). Subsequently, both samples were temporarily deformed into a rolled shape and cooled in ice water to fix their temporary form. Upon reheating in hot water, the reprogrammed sample recovered its helical shape, while the control sample returned to its original strip configuration (Fig. 7b and Movie S4). These results indicate that excellent shape-memory behaviour is preserved even after permanent reprogramming. Finally, the sample initially reprogrammed from a flat strip to a helical shape was further reprogrammed into a ring-like permanent configuration. Remarkably, this new permanent shape also maintained outstanding shape-memory properties, underscoring the material's robustness and its ability to sustain functional performance through multiple shape reprogramming cycles (Fig. 7c and Movie S5).

3. Conclusions

In this study, we successfully developed reprogrammable shape memory ion gels consisting of UHMW PMMA and the IL [C_2mim][NFSI] through a facile one-pot polymerisation. The resulting ion gel exhibited a high T_g above room temperature, accompanied by a broad rubbery plateau, which can be attributed to the abundant entanglement of UHMW PMMA chains within IL. A key advantage of this system lies in its ability to finely tune T_g by simply adjusting the polymer/IL ratio and selecting different IL structures, offering a versatile platform for the design of shape memory materials with tailored properties. DMA and uniaxial tensile tests confirmed the excellent mechanical strength, recyclability, and outstanding shape-memory properties of the ion gel, including triple shape-memory behaviour. Moreover, cyclic shape memory tests revealed that the UHMW PMMA/[C_2mim][NFSI] ion gel maintained its shape-memory capabilities even after multiple deformation cycles, with negligible residual strain. In contrast, composites with lower molecular weight PMMA showed incomplete shape recovery due to polymer chain pullout, highlighting the critical role of chain entanglement in achieving exceptional shape-memory performance. In addition to shape-memory capabilities–such as thermally-triggered actuation under load and shape transformation–permanent shape reprogramming was achieved through thermal relaxation of physical entanglements, further showcasing the potential of the developed ion gel for various smart applications. Overall, our results show that a densely entangled UHMW PMMA/[C_2mim][NFSI] ion gel enables permanent shape reprogramming *via* thermal equilibration driven by entanglement relaxation, while retaining its triple-shape memory, recyclability, and strain-sensing capabilities, thereby providing a versatile platform for advanced shape-memory materials.

The strategy reported in this study is not limited to ion-gel systems and is expected to be applicable to a wide range of polymer systems. In recent years, several studies have described the synthesis of UHMW polymers *via* controlled polymerisation techniques.[19,66–69] In addition, we have recently demonstrated that UHMW gels can be formed *via in situ* polymerisation even in highly concentrated organic electrolyte systems.[45] Building on these findings, extending the present strategy to other polymer material systems represents an important direction for future research. Furthermore, beyond molecular weight, fundamental investigations into the effects of polymer structural parameters, such as molecular weight distribution and branching architecture, will be necessary to achieve a more comprehensive understanding of structure–property relationships in these systems. Our results would open new avenues for designing reprogrammable shape memory materials based entirely on physical entanglements.

4. Experimental section

4.1. Materials

Methyl methacrylate (MMA) was purchased from TCI (Japan) and purified by passing it through activated alumina. The thermal radical polymerisation initiator, 2,2′-azobis(2,4-dimethylvaleronitrile) (V-65), was purchased from Fujifilm Wako Pure Chemical Corporation (Japan) and used as received. 1-Ethyl-3-methylimidazolium bromide ([C_2mim]Br) was purchased from TCI, and potassium bis(nonafluorobutanesulfonyl)imide (KNFSI) was obtained from Mitsubishi Materials Electronic Chemicals Co., Ltd (Japan). 1-Ethyl-3-methylimidazolium bis(trifluoromethanesulfonyl)imide ([C_2mim][TFSI]) was purchased from Kishida Chemical Co., Ltd (Japan) and used as received.

4.2. Synthesis of [C_2mim][NFSI]

1-Ethyl-3-methylimidazolium bis(nonafluorobutanesulfonyl)imide ([C_2mim][NFSI]) was synthesised *via* a metathesis reaction between [C_2mim]Br and KNFSI as described below. [C_2mim]Br (10.0 g, 52.3 mmol) and KNFSI (29.2 g, 47.1 mmol) were dissolved in 45 mL of ethanol and stirred at 60 °C overnight. The resulting precipitate, KBr, was filtered off, and ethanol was removed using a rotary evaporator. The residue was then washed five times with distilled water. The recovered oil phase was stirred under vacuum at room temperature overnight, followed by further vacuum drying at 80 °C to obtain the desired oily product, [C_2mim][NFSI] (yield: 43%).

4.3. Synthesis of PMMA/[C_2mim][NFSI] composites

The composite of PMMA and [C_2mim][NFSI] was prepared *via in situ* radical polymerisation of MMA in [C_2mim][NFSI], following a previously reported method.[42] As a representative procedure, the synthesis of 45wt-PMMA-H-[C_2mim][NFSI] is described below. The MMA monomer (0.940 g, 9.4 mmol), [C_2mim][NFSI] (1.15 g, 1.7 mmol), and initiator V-65 (0.466 mg, 1.8 μmol) were mixed in a vial to form a transparent precursor solution, which was bubbled with argon for 15 min at room temperature. The solution was then transferred to a mould composed of two PET films with a silicone rubber spacer, sealed inside a glovebox ([O_2] < 1 ppm, [H_2O] < 1 ppm), and polymerised at 70 °C for 24 h to obtain a PMMA/[C_2mim][NFSI] composite sheet.

The molecular weight of PMMA in the composite was determined by completely dissolving the composite in acetone, followed by purification of PMMA through reprecipitation *via* dropwise addition into an excess amount of methanol. The obtained PMMA was dissolved in a 10-mM lithium bromide/*N*,*N*-dimethylformamide solution, used as the eluent, and analysed using a gel permeation chromatography (GPC) system (Shimadzu, Japan). The molecular weight and molecular weight distribution were determined based on a calibration curve prepared using PMMA standards.

4.4. Rheological measurements

Temperature sweep measurements were conducted using an MCR102 rheometer (Anton Paar, Austria) with a parallel plate geometry of 8 mm in diameter. Measurements were performed from 0 to 180 °C at a heating rate of 1 °C min^{-1}, a frequency rate of 1 rad s^{-1}, and a strain amplitude of 1%.

The viscoelastic master curve was constructed using an ARES-G2 rheometer (TA Instruments, USA) equipped with an ACS3 chiller. An 8 mm cross-hatched plate was used as the upper plate and a 40 mm cross-hatched plate was used as the lower plate. The master curve was constructed by performing frequency sweep measurements at different temperatures ranging from 40 to 200 °C and shifting the data according to the time-temperature superposition principle. Frequency sweeps at each temperature were performed over an angular frequency range of 0.1–100 rad s^{-1}. The strain amplitude was initially set to 0.01% at 40 °C and was incrementally increased during the measurements to compensate for the reduction in torque caused by the stiffness change across the glass transition.

Relaxation spectra were obtained in TRIOS software by converting the viscoelastic master curves using nonlinear regularization fitting. The obtained relaxation spectra were fitted with a Gaussian function defined as a function of the logarithm of the relaxation time.[70] Deconvolution of the fitted spectra resolved three relaxation components, comprising two peaks independent of molecular weight and one peak dependent on molecular weight. The former were associated with the glass transition, whereas the latter was assigned to terminal relaxation.

4.5. Differential scanning calorimetry (DSC)

DSC measurements were performed using a Discovery DSC 250 (TA Instruments, USA). The samples were cooled to −120 °C, heated to 200 °C, cooled again to −120 °C, and then reheated to 200 °C at cooling and heating rates of 10 °C min^{-1}. Modulated DSC (MDSC) measurements were conducted after the conventional DSC runs. For MDSC, the samples were heated at 2.5 °C min^{-1} with a modulation amplitude of ±1 °C and a period of 60 s.

4.6. Dynamic mechanical analysis (DMA)

To evaluate the shape memory properties of the composites, dynamic mechanical analysis (DMA) was performed using a Discovery DMA 850 equipped with a liquid nitrogen cooling accessory (TA Instruments, USA). The sample was cut into a rectangular shape with a length of 20–25 mm and a width of 5–6 mm, then set in the DMA apparatus with a clamp length of approximately 5 mm. The temperature was increased from room temperature to 60 °C, followed by equilibration for 5 min. A strain of 100% was then applied to the sample at a stretching rate of 100% min^{-1}. While maintaining this strain, the sample was cooled from 60 to 0 °C at a cooling rate of 5.0 °C min^{-1} and subsequently equilibrated at 0 °C for 5 min. Finally, the stress was set to 0.0 Pa, and the temperature was increased from 0 to 100 °C at a heating rate of 3.0 °C min^{-1}.

The shape fixation ratio (R_f) and shape recovery ratio (R_r) of the composites were evaluated using the following equations:

$$R_f = \varepsilon_u\ (T = 0\ ^\circ C)/\varepsilon_m$$

$$R_r = (\varepsilon_m - \varepsilon_u\ (T = 100\ ^\circ C))/\varepsilon_m$$

where ε_u (T) represents the strain in the stress-free state at temperature T, and ε_m denotes the applied maximum strain, which is set to ε_m = 100% in this experiment.

4.7. Tensile tests

Tensile test samples were prepared by punching dumbbell-shaped specimens (JIS K 6251 No. 7, rectangular portion size: 2 mm × 12 mm × 0.25 mm) from the synthesised composite sheets. Uniaxial tensile tests were conducted using an AGX tester (Shimadzu, Japan) at a tensile speed of 100 mm min^{-1}. The changes in mechanical properties during repeated shape memory cycles were evaluated by stretching the sample to 150% strain and then returning to the 0% loading position, followed by shape recovery through heat treatment at 100 °C in an oven for 1 min. This process was repeated five times, and changes in the stress–strain curves were examined. Additionally, the residual strain was evaluated by comparing the sample length before and after the cycling shape memory tests.

4.8. Electrochemical measurements

Electrochemical properties of ion gels were evaluated using a VMP3 potentiostat/galvanostat (Bio-Logic Science Instruments, France). Ionic conductivity was measured by electrochemical impedance spectroscopy (EIS) over a frequency range of 0.1 Hz to 1 MHz with an AC amplitude of 10 mV. The sample was sandwiched between two stainless steel disk electrodes and measurements were conducted over a temperature range of 20–100 °C.

The resistance change upon tensile deformation was evaluated by EIS under strain using a dumbbell-shaped specimen (JIS K 6251 No. 6; rectangular gauge section: 4 mm × 25 mm × 0.5 mm). Conductive tape electrodes were attached to the rectangular gauge section, and impedance spectra were recorded while applying tensile strain. The bulk resistance (R_{bulk}, hereafter denoted as R) was determined from the Nyquist plots. The bulk resistance at each strain was obtained, and the difference from the resistance at zero strain (R_0) was defined as $\Delta R = R - R_0$. The relative resistance change, $\Delta R/R_0$, was then evaluated as a function of strain.

Author contributions

R. T.: conceptualization, data curation, funding acquisition, investigation, project administration, resources, visualization, writing – original draft. K. U.: conceptualization, data curation, investigation, resources, visualization, writing – review & editing. Y. K.: conceptualization, data curation, investigation, writing – review & editing. T. U.: conceptualization, writing – review & editing.

Conflicts of interest

R.T., K.U., and T.U. are inventors on pending patent applications filed by the National Institute for Materials Science (JP patent application no. 2023-209262, filed on 12 December 2023). Y.K. declares that he has no competing interests.

Data availability

The data supporting this article have been included as part of the supplementary information (SI). See DOI: https://doi.org/10.1039/d5mh01902h.

Acknowledgements

This work was financially supported by JSPS KAKENHI (23K26409 to R.T. and 23H02030 to T. U.), JST PRESTO program (JPMJPR2196 to R.T.), and JST FOREST Program (JPMJFR2327 to K.U.).

Notes and references

1 H. Meng and G. Li, *Polymer*, 2013, **54**, 2199–2221.
2 D. Habault, H. Zhang and Y. Zhao, *Chem. Soc. Rev.*, 2013, **42**, 7244–7256.
3 W. M. Huang, B. Yang, Y. Zhao and Z. Ding, *J. Mater. Chem.*, 2010, **20**, 3367.
4 J. Thévenot, H. Oliveira, O. Sandre and S. Lecommandoux, *Chem. Soc. Rev.*, 2013, **42**, 7099–7116.
5 A. Lendlein, H. Jiang, O. Jünger and R. Langer, *Nature*, 2005, **434**, 879–882.
6 Q. Ze, X. Kuang, S. Wu, J. Wong, S. M. Montgomery, R. Zhang, J. M. Kovitz, F. Yang, H. J. Qi and R. Zhao, *Adv. Mater.*, 2020, **32**, e1906657.
7 R. Sanaka, S. K. Sahu, P. S. R. Sreekanth, K. Senthilkumar, N. D. Badgayan, B. V. Siva and Q. Ma, *J. Compos. Sci.*, 2024, **8**, 324.
8 L. Luo, F. Zhang, L. Wang, Y. Liu and J. Leng, *Adv. Funct. Mater.*, 2024, **34**, 2312036.
9 A. Lendlein and O. E. C. Gould, *Nat. Rev. Mater.*, 2019, **4**, 116–133.

10 F. Pilate, A. Toncheva, P. Dubois and J.-M. Raquez, *Eur. Polym. J.*, 2016, **80**, 268–294.
11 Y. Xia, Y. He, F. Zhang, Y. Liu and J. Leng, *Adv. Mater.*, 2021, **33**, 2000713.
12 W. Zhao, C. Yue, L. Liu, Y. Liu and J. Leng, *Adv. Healthcare Mater.*, 2023, **12**, e2201975.
13 M. Zarek, M. Layani, I. Cooperstein, E. Sachyani, D. Cohn and S. Magdassi, *Adv. Mater.*, 2016, **28**, 4449–4454.
14 C. M. Yakacki and K. Gall, *Shape-Memory Polymers*, Springer, Berlin Heidelberg, 2010.
15 K. Uto, Y. Liu, M. Mu, R. Yamamoto, C. Azechi, M. Tenjimbayashi, A. Kaeser, M.-A. Marliac, M. M. Alam, J. Sasai and M. Ebara, *Adv. Mater. Interfaces*, 2024, **11**, 2300274.
16 X. Zheng, Y. Chen, C. Chen, Z. Chen, Y. Guo, H. Li and H. Liu, *J. Mater. Chem. B*, 2021, **9**, 7371–7380.
17 A. Lendlein, M. Behl, B. Hiebl and C. Wischke, *Expert Rev. Med. Devices*, 2010, **7**, 357–379.
18 H. Gao, J. Li, F. Zhang, Y. Liu and J. Leng, *Mater. Horiz.*, 2019, **6**, 931–944.
19 A. Lendlein and S. Kelch, *Angew. Chem., Int. Ed.*, 2002, **41**, 2034.
20 C. Liu, H. Qin and P. T. Mather, *J. Mater. Chem.*, 2007, **17**, 1543.
21 I. A. Rousseau, *Polym. Eng. Sci.*, 2008, **48**, 2075–2089.
22 K. Uto, Y. Matsushita and M. Ebara, *Polym. Chem.*, 2023, **14**, 1478–1487.
23 M. Ebara, K. Uto, N. Idota, J. M. Hoffman and T. Aoyagi, *Adv. Mater.*, 2012, **24**, 273–278.
24 K. Nagahama, Y. Ueda, T. Ouchi and Y. Ohya, *Biomacromolecules*, 2009, **10**, 1789–1794.
25 T. Xie, *Nature*, 2010, **464**, 267–270.
26 C. Samuel, S. Barrau, J.-M. Lefebvre, J.-M. Raquez and P. Dubois, *Macromolecules*, 2014, **47**, 6791–6803.
27 Q. Zhao, M. Behl and A. Lendlein, *Soft Matter*, 2013, **9**, 1744–1755.
28 H. Chen, Y. Li, G. Tao, L. Wang and S. Zhou, *Polym. Chem.*, 2016, **7**, 6637–6644.
29 T. Ware, K. Hearon, A. Lonnecker, K. L. Wooley, D. J. Maitland and W. Voit, *Macromolecules*, 2012, **45**, 1062–1069.
30 J. Odent, J.-M. Raquez, C. Samuel, S. Barrau, A. Enotiadis, P. Dubois and E. P. Giannelis, *Macromolecules*, 2017, **50**, 2896–2905.
31 C. Liu, S. B. Chun, P. T. Mather, L. Zheng, E. H. Haley and E. B. Coughlin, *Macromolecules*, 2002, **35**, 9868–9874.
32 J. Zhao, M. Chen, X. Wang, X. Zhao, Z. Wang, Z.-M. Dang, L. Ma, G.-H. Hu and F. Chen, *ACS Appl. Mater. Interfaces*, 2013, **5**, 5550–5556.
33 K. Wang, Y.-G. Jia and X. X. Zhu, *Macromolecules*, 2017, **50**, 8570–8579.
34 S. Basak, *Smart Mater. Res.*, 2024, **1**, 48.
35 X. Gu and P. T. Mather, *Polymer*, 2012, **53**, 5924–5934.
36 K. Sakurai and T. Takahashi, *J. Appl. Polym. Sci.*, 1989, **38**, 1191–1194.
37 G. B. Kauffman, S. W. Mason and R. B. Seymour, *J. Chem. Educ.*, 1990, **67**, 198.
38 R. Zhang, Q. Yang, M. Liu, X. Chen and P. Xue, *Mater. Lett.*, 2022, **325**, 132813.
39 A. Maksimkin, S. Kaloshkin, M. Zadorozhnyy and V. Tcherdyntsev, *J. Alloys Compd.*, 2014, **586**, S214–S217.
40 K. Inomata, K. Nakagawa, C. Fukuda, Y. Nakada, H. Sugimoto and E. Nakanishi, *Polymer*, 2010, **51**, 793–798.
41 J. D. Marquez, K. A. Stewart, K. C. Stevens, B. J. Ryder, T. H. Le, N. B. Wei, W. J. Choi, Y. Huang, B. S. Sumerlin and A. M. Evans, *J. Am. Chem. Soc.*, 2025, **147**, 29223–29231.
42 Y. Kamiyama, R. Tamate, T. Hiroi, S. Samitsu, K. Fujii and T. Ueki, *Sci. Adv.*, 2022, **8**, eadd0226.
43 Y. Kamiyama, R. Tamate, K. Fujii and T. Ueki, *Soft Matter*, 2022, **18**, 8582–8590.
44 R. Tamate, Y. Kamiyama and K. Kojio, *Small*, 2025, **21**, e09922.
45 Y. Kamiyama, T. Ueki and R. Tamate, *Soft Matter*, 2025, **21**, 1471–1478.
46 J. Liu, G. Li, H. Liu, J. Wang, H. Wang, X. Gao, Q. Liu and C. Wang, *J. Bionic Eng.*, 2024, **21**, 1397–1411.
47 T. Hada, Y. Komagamine, M. Kanazawa and S. Minakuchi, *J. Prosthodont. Res.*, 2024, **68**, 181–185.
48 J. Li, T. Liu, Y. Pan, S. Xia, Z. Zheng, X. Ding and Y. Peng, *Macromol. Chem. Phys.*, 2012, **213**, 2246–2252.
49 C. Samuel, S. Barrau, J.-M. Lefebvre, J.-M. Raquez and P. Dubois, *Macromolecules*, 2014, **47**, 6791–6803.
50 C. E. Porter and F. D. Blum, *Macromolecules*, 2000, **33**, 7016–7020.
51 Z. Jiang, C. T. Imrie and J. M. Hutchinson, *Thermochim. Acta*, 2002, **387**, 75–93.
52 J. Wu, G. Huang, L. Qu and J. Zheng, *J. Non-Cryst. Solids*, 2009, **355**, 1755–1759.
53 S. G. M. van Lange, D. W. te Brake, E. F. Brink, J. Pees, M. M. van Nieuwenhuijzen, N. Vengallur, A. Zaccone, A. Giuntoli, J. Sprakel and J. van der Gucht, *Nat. Commun.*, 2026, **17**, 1374.
54 M. L. Ferreira, M. J. Pastoriza-Gallego, J. M. M. Araújo, J. N. Canongia Lopes, L. P. N. Rebelo, M. M. Piñeiro, K. Shimizu and A. B. Pereiro, *J. Phys. Chem. C*, 2017, **121**, 5415–5427.
55 M. L. Thomas, Y. Oda, R. Tatara, H.-M. Kwon, K. Ueno, K. Dokko and M. Watanabe, *Adv. Energy Mater.*, 2017, **7**, 1601753.
56 J. P. Hallett and T. Welton, *Chem. Rev.*, 2011, **111**, 3508–3576.
57 L. H. Sperling, *Introduction to Physical Polymer Science*, Wiley Interscience, 2005.
58 J. J. Benkoski, G. H. Fredrickson and E. J. Kramer, *J. Polym. Sci. B Polym. Phys.*, 2002, **40**, 2377–2386.
59 Z. Luo, W. Li, J. Yan and J. Sun, *Adv. Funct. Mater.*, 2022, **32**, 2203988.
60 T. Ueki and M. Watanabe, *Macromolecules*, 2008, **41**, 3739–3749.
61 M. P. Scott, M. Rahman and C. S. Brazel, *Eur. Polym. J.*, 2003, **39**, 1947–1953.
62 M. M. Mok, X. Liu, Z. Bai, Y. Lei and T. P. Lodge, *Macromolecules*, 2011, **44**, 1016–1025.

63 S. Kim, S.-W. Lee, H. Kwon, S. Hong, G. Kim, S. M. Tawfik, H. W. Park and H. E. Jeong, *Adv. Funct. Mater.*, 2026, **36**, e16218.
64 M. Behl and A. Lendlein, *J. Mater. Chem.*, 2010, **20**, 3335.
65 Q. Zhao, W. Zou, Y. Luo and T. Xie, *Sci. Adv.*, 2016, **2**, e1501297.
66 R. N. Carmean, T. E. Becker, M. B. Sims and B. S. Sumerlin, *Chem*, 2017, **2**, 93–101.
67 R. N. Carmean, M. B. Sims, C. A. Figg, P. J. Hurst, J. P. Patterson and B. S. Sumerlin, *ACS Macro Lett.*, 2020, **9**, 613–618.
68 Z. An, *ACS Macro Lett.*, 2020, **9**, 350–357.
69 J. D. Marquez, G. Otgonjargal, K. A. Stewart, A. M. M. Hasan, G. C. Gilchrist, B. S. Sumerlin and A. M. Evans, *Chem. Mater.*, 2025, **37**, 9985–9992.
70 V. Montano, S. J. Picken, S. Van Der Zwaag and S. J. Garcia, *Phys. Chem. Chem. Phys.*, 2019, **21**, 10171–10184.